

Article

DNN Beamforming for LEO Satellite Communication at Sub-THz Bands

Rajnish Kumar ^{*,†}  and Shlomi Arnon [†] 

Department of Electrical and Computer Engineering, Faculty of Engineering Sciences, Ben-Gurion University of the Negev, Beer-Sheva 8410501, Israel

* Correspondence: rajnish@post.bgu.ac.il

† These authors contributed equally to this work.

Abstract: The 6G communication system will be designed at sub-THz frequencies due to increasing demand in data rates, emerging new applications and advanced communication technologies. These high-performing systems will heavily rely on artificial intelligence (AI) for efficient and robust design of transceivers. In this work, we propose a deep neural network (DNN) beamformer that will replace the use of phase shifters for a massive array of antenna elements employed at the ground station for wideband LEO satellite communication at sub-THz bands. We show that the signal processing algorithm employed using DNN is capable to match the performance of a true-time delay beamformer as the angle of arrival of the received wideband signal at the ground station is changing due to rapid movement of the LEO satellite. The implementation of DNN beamformer will be able to reduce the cost of receiver and provide a way for the efficient and compact design of the massive array beamforming for wideband LEO satellite applications.

Keywords: beamforming; deep neural network; LEO satellite; sub-THz bands



Citation: Kumar, R.; Arnon S. DNN Beamforming for LEO Satellite Communication at Sub-THz Bands. *Electronics* **2022**, *11*, 3937. <https://doi.org/10.3390/electronics11233937>

Academic Editors: Min Jia, Zhenyu Na, Xin Liu and Lexi Xu

Received: 27 October 2022
Accepted: 25 November 2022
Published: 28 November 2022

Publisher's Note: MDPI stays neutral with regard to jurisdictional claims in published maps and institutional affiliations.



Copyright: © 2022 by the authors. Licensee MDPI, Basel, Switzerland. This article is an open access article distributed under the terms and conditions of the Creative Commons Attribution (CC BY) license (<https://creativecommons.org/licenses/by/4.0/>).

1. Introduction

The next generation of communication systems (B5G and 6G) will extensively rely on artificial intelligence (AI) for the efficient and robust design of transceiver systems. These transceiver systems will be designed at sub-THz bands to achieve higher spectral efficiency, data rate and energy efficiency [1]. The lower frequency bands are also congested so the communication systems, new emerging applications and devices are to be designed at higher frequency bands [2]. The system design at sub-THz bands will enable many new services beyond 5G with enhanced security and frequency reuse. The existing 5G NR has already been planned to complement the non-terrestrial networks (NTN) to provide access to the remote locations. In its release 15 [3], 3GPP studied the scenario of the New Radio (NR) to support the Non-Terrestrial Network (NTN). The NTN refer to the satellite, high altitude platforms, air-to-ground networks. The study identified the role of NTN to support the Transportation, Safety, eHealth, Agriculture, Finance, Automotive, Entertainment Media and Energy. The services enabled by the NTN integrated with the Terrestrial network include the eMBB (enhanced Mobile Broadband) and mMTC (massive Machine Type Communications). The Release 16 Study of 3GPP focused on adapting the NR systems to support NTN by minimizing the need for new interfaces and protocols [4]. The Release 17 study focuses on providing support of Narrow-Band Internet of Things (NB-IoT) and enhanced Machine Type Communication (eMTC) based satellite access [5]. These satellite networks have been assumed to have the beam steering capabilities towards the users on the ground using beamforming techniques [6].

As the communication system will evolve into the future generation e.g., B5G and 6G, the NTN will be integrated into the densely connected communication network coherently to provide cost effective services, better network capacity and coverage with higher energy efficiency [7,8]. The larger available bandwidth at sub-THz bands will lead to a wideband communication system with very high data rates. However, the design of communication

system at such higher frequencies poses unique set of challenges [9]. Such challenges include the beamforming and antenna array design [10–12], channel modelling and estimation, massive MIMO communication [13] along with novel modulation techniques and signal processing algorithm [14,15].

Several LEO satellite constellations have been launched, e.g., Starlink, OneWeb, Globalstar, Orbcomm to provide access and connectivity to remote and unconnected areas. There are planned launches in 2023 by the Project Kuiper of Amazon [16]. The Lynk Global satellite that is expected to provide satellite-to-mobile-phone connectivity will deploy its 5G payload sooner rather than later [17]. Emergency SOS via satellite, a feature provided in iPhone-14 will connect to satellite in case of non-availability of cellular and Wi-Fi networks [18]. Such developments show the growing importance of the LEO communication in providing global services and connectivity. These LEO constellations will provide the communication services with lower latency due to faster propagation in free-space with thousands of satellites in the orbit [19].

For the design of satellite links at the higher frequencies in sub-THz bands (100–300 GHz), one such challenge to system design consideration comes due to higher absorption loss of the propagating signal in the atmospheric channel. In addition, the rapid movement of LEO satellites require phased array antenna at the ground station for electronic beam steering that can be pointed to a desired direction in real time [20,21]. The higher losses due to the atmospheric absorption can be compensated by using very large number of antenna elements that employ beamforming to form very narrow pencil beams in order to achieve very high gain in the desired direction [22,23]. The shorter wavelength allows the design of very small antennas that can be densely packaged as massive phased arrays of antenna elements. However, as we move to higher frequency bands above 100 GHz, the use of phase shifters for beamforming for a wideband system at sub-THz is less recommended due to inefficiency, non-linearity and beam squinting effects [24,25].

Currently, the design of phased array antenna mostly rely on use of phase shifters for analog beamforming of the receiver of the massive array of elements that will cause beam squinting problem especially for large bandwidth communication system [26]. For a wideband system, this could degrade the performance significantly. The phase shifters are also not efficient for attaining wide scanning angles [26,27]. The alternative option to phase shift beamforming is the use of true-time delay (TTD) analog beamforming though its implementation is costly. Furthermore, a very large number of antenna elements employed at the receiver will significantly increase the cost of implementation with such analog processing of antenna array output signals. To resolve these issues, one option is to implement digital beamforming that will require some additional components in the front end design of wideband receiver. However, thanks to the breakthrough advancements in digital integrated circuits and technology, it is now becoming more affordable and with digital processing, it is a lot easier to put into practice [28,29].

In this work, to address the aforementioned problems, we propose to implement the beamforming algorithm of the massive number of receiver antenna elements using a deep neural network (DNN). The output of individual array elements are fed into a deep neural network through an analog to digital converter (ADC) and the DNN beamformer is trained to mimic the actual output voltage generated by a TTD beamformer as the angle of arrival (AoA) changes at the receiver due to rapid movement of the LEO satellite. The numerical results show that DNN beamforming algorithm is able to match the voltage output of a TTD beamformer with a very low mean square error for a wideband signal. Such implementation of the signal processing algorithm will reduce the cost of receiver and various nonidealities caused by the phase shifter beamformer as we employ a massive array of antenna elements for the receiver design at sub-THz bands. To the best knowledge of the authors, the proposed beamforming algorithm using the novel deep learning algorithm for wideband LEO satellite applications at sub-THz bands is for the first time to be published.

2. DNN Beamforming

The LEO satellite moves at very high velocity in its orbit and hence the angle of arrival at the ground station receiver is constantly changing. The transmitted signals from the satellite that arrive at the ground station based phased array elements have different delays at the array output and thus has to be combined in such a way that there is a constructive interference at the beamformer output. Each antenna element is thus provided a phase shifter that delays the signal accordingly to get a constructive interference. However, the performance of phase shifter would degrade as the frequency of arriving signal changes and thus the spacing between antenna elements would change in terms of wavelength. This will lead to the problem of beam squinting [30] that would cause significant degradation in the performance of massive array receiver for a wideband system. Moreover, massive antenna array design will also require very large number of phase shifters for phased array receiver thus raising the cost of implementation much higher.

To avoid these problems due to phase shifters, true-time delay can be employed at each of the array elements but it will be a costly implementation due to massive number of antenna elements used for beamforming. The true-time delay provides exact time delay needed at the output of each antenna elements for providing a constructive interference at the output. Therefore, we propose to perform the signal processing of the received signal at each antenna elements by a DNN beamforming algorithm. Recently deep learning and machine learning algorithm has helped improved the system performance in many scenarios and diverse range of applications [31–33]. Such an algorithm, that is mainly data-driven once trained, can be deployed in real-time applications for the prediction, optimization and management of scarce communication resources. It has been successfully implemented to improve the performance of signal processing algorithms [34,35], design of intelligent communication systems [36], optimization of satellite resources and its allocation [37]. The data-driven DNN algorithms have also been applied in obtaining hybrid beamforming to solve spectral efficiency maximization problems [38], optimization of downlink beamforming [39], and the support of highly mobile systems [40].

In our proposed algorithm, the DNN is trained such that it minimizes the error in the predicted output voltage by tracking the output voltage of a TTD beamformer as the AoA at the receiver changes due to movement of LEO satellite. In Figure 1, we show the schematic of phase shift beamforming and the DNN beamforming for the phased array antenna receiver based at the ground station for a given AoA θ_0 .

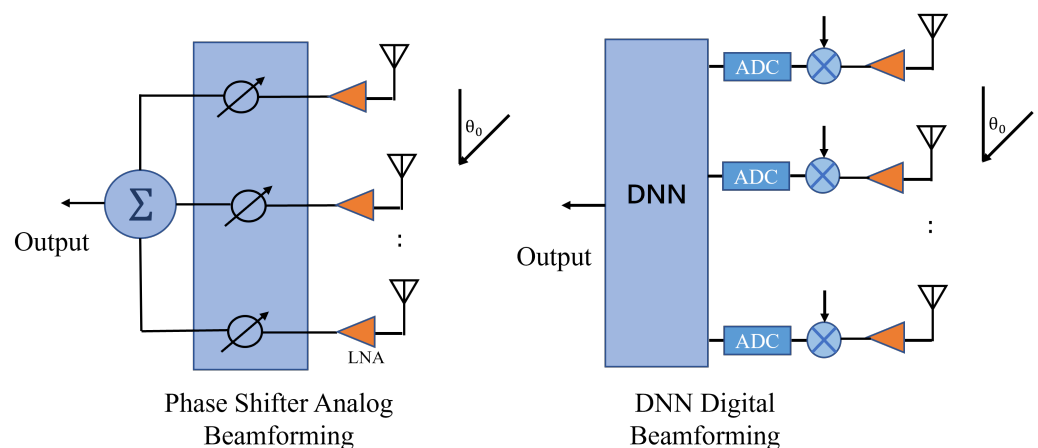


Figure 1. Schematic of Phase shift and DNN Beamforming.

For a uniform linear array of isotropic radiators receiver, the signal voltage at the array output will be expressed as [41]

$$V_{out} = \sum_{n=1}^N V_n e^{-j\frac{2\pi d}{\lambda}(n-1)\cos\theta_0} \tag{1}$$

where d is the spacing between the array elements, λ is the wavelength, N is the number of array elements, θ_0 is the angle of arrival of signal at the antenna elements measured from local zenith, and V_n is the signal amplitude at n th element.

Assuming the plane wave at the receiver with uniform illumination of the array elements, we can express the signal amplitude at the array elements as

$$V_n = \sqrt{\frac{\eta_T \eta_R P_T G_T}{L_{FS}(\theta_0) L_A(\theta_0)}} \quad (2)$$

where η_T and η_R are the efficiencies of transmitting and receiving antennas respectively, P_T is the transmitted power, G_T is the gain of transmitting antenna, $L_{FS}(\theta_0)$ is the free-space path loss, and $L_A(\theta_0)$ is the absorption loss in the atmosphere for a given AoA at the ground station.

The losses are dependent on the AoA of the signal at the receiver as the slant path length changes due to movement of LEO satellite. The free-space path loss as a function of AoA is given by [24]

$$L_{FS}(\theta_0) = \left(\frac{4\pi}{\lambda}\right)^2 \left[-R_0 \cos \theta_0 + \sqrt{(R_0 + h_s)^2 - R_0^2 \sin^2 \theta_0}\right]^2 \quad (3)$$

where $R_0 = 6371$ km (the radius of the earth) and h_s is the altitude of LEO satellite.

The absorption losses over the atmospheric channel depends on many factors including the frequency, gaseous constituents, pressure, temperature, humidity and the slant path length through the atmospheric media. The atmospheric loss can be calculated by considering the atmospheric media as several homogeneous layers of gases and calculating the specific attenuation and path length through each layer. The atmospheric absorption loss of the signal can be expressed as [42]

$$L_A(\theta_0) = \sum_{i=1}^L \gamma_i d_i(\theta_0) \quad (4)$$

where L is the number of homogeneous layers of atmospheric media, γ_i is the specific attenuation of each of such layer, and $d_i(\theta_0)$ is the slant path length through each layer for a given AoA θ_0 .

The proposed DNN beamformer has to be trained in order to mimic the performance of a TTD beamformer so that we need to compute the output voltage of a TTD beamformer to train the network in a supervised manner. The output voltage of the TTD beamformer can be expressed as

$$V_{out}^{TTD} = \sum_{n=1}^N V_n e^{-j\left[\frac{2\pi d}{\lambda}(n-1) \cos \theta_0 - 2\pi f \tau_n\right]} \quad (5)$$

where τ_n is the time delay provided at the n th antenna element. These delay elements have to provide a time delay of $(n-1)(d/c) \cos \theta_0$ at the n th antenna element for a constructive interference at the output with no beam squinting problem as occurs with phase shift beamforming.

For the phase shift beamformer (PSB), the signal voltage at the output of phase shifter network of antenna array can be expressed as

$$V_{out}^{PSB} = \sum_{n=1}^N V_n e^{-j\left[\frac{2\pi d}{\lambda}(n-1) \cos \theta_0 - \frac{2\pi d}{\lambda_0}(n-1) \cos \theta_0\right]} \quad (6)$$

where λ is the wavelength of the signal arriving at the array elements in the direction of θ_0 and λ_0 is the center frequency at which the phase shifter is designed to provide a phase shift for constructive interference of the signals. We note that when the arriving signal have a frequency of c/λ_0 , we get unity gain in the direction of θ_0 while as the signal frequency deviates, there will be degradation in the gain of beamforming array.

For the DNN beamformer, we provide the input to the network as the output voltage amplitude of each of the array elements through an ADC and the output of DNN is the combined voltage signal that is trained to mimic the output of a TTD beamformer. The schematic of DNN beamformer is presented in Figure 2 showing the array elements voltages through ADC fed into the network that is combined to produce a regression output voltage. The input to the each of the neurons in the first layer will be expressed as [43]

$$f(X) = \sum_{i=1}^n W_i^1 V_i + b_1 \tag{7}$$

where W_i^1 is the weight matrix for a neuron in the first hidden layer, V_i is the column vector of the voltages obtained from individual antenna array elements, n is the total number of array elements employed, and b_1 is the bias for the first hidden layer.

The input received to each neuron is then passed through an activation function such that the output of the neuron can be expressed as

$$g(X) = \sigma(f(X)) \tag{8}$$

where σ is the sigmoid function.

The output of this first layer of neurons are then fed as the input to the second layer of neurons and so on. The calculation can be repeated for any given number of layers and the output of beamformer V_{out}^{DNN} can be evaluated. The output voltage of the DNN beamformer is implemented by a linear activation function and thus can be expressed as

$$V_{out}^{DNN} = \sum_{m=1}^M W_m^l g_m^l(X) \tag{9}$$

where $g_m^l(X)$ is the output from last hidden layer l , W_m^l is the weights associated with these outputs, and M is the number of neurons in the last hidden layer.

In order to learn the parameters of the DNN beamformer, we need to define a loss function that will be minimized by the training algorithm [44]. We define the empirical loss function to train the network as

$$\text{Loss} = \frac{1}{K} \sum_{k=1}^K (V_{out}^{TDD} - V_{out}^{DNN})^2 \tag{10}$$

where V_{out}^{TDD} and V_{out}^{DNN} are the array output voltage with TTD and DNN beamformer respectively, and K is the number of training samples. Our objective is to minimize this loss function by finding the parameters of the DNN beamformer that includes its weights and biases.

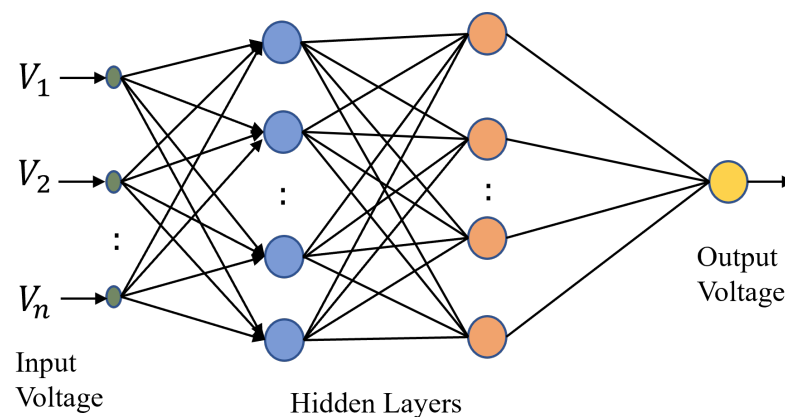


Figure 2. Schematic of the DNN Beamforming with input being fed by the voltages from individual array antenna elements.

To summarize, the algorithm takes the input from the output of ADC network of the massive antenna array i.e., (V_1, V_2, \dots, V_n) . Once the input is obtained, it is passed to the neural network with several layers of neurons and the output of neural net V_{out}^{DNN} is obtained. With the obtained output, we compute the loss (as defined in (10)) with respect to the TTD beamformer V_{out}^{TTD} and then use backpropagation algorithm to update the weights and biases of the network for all the training samples. Once trained, we deploy the DNN beamformer to predict for many test samples and to test its accuracy in matching the performance close to the TTD beamformer.

3. Numerical Results

The parameters for performing the numerical simulation are mentioned in Table 1. In order to calculate the atmospheric losses due to gases at an angle of arrival θ_0 , we have used the ITU recommendation by considering a multi-layered homogeneous atmosphere with total of $L = 922$ layers and a total height of 100 km [42]. The recommendation P.676-13 [42] provides the method to compute the absorption loss due to the gaseous atmosphere for the frequency range upto 1000 GHz. The major contributor is the oxygen and water vapor. The reference standard atmosphere as given in the ITU recommendation P.835-6 [45] provide the atmospheric models to be used in the computation of gaseous absorption loss along the Earth–space paths. It provides the calculation of atmospheric parameters i.e., pressure, temperature and water vapor density as a function of height. In order to calculate the pressure, temperature and water vapor profile of the standard atmosphere model, we assume the mean annual global reference atmosphere as given in ITU recommendation [45], which is the most commonly used model [24,46]. We consider the bandwidth of the signal to be 2 GHz at a center frequency of 100 GHz and the signal occupying the frequency range of 99–101 GHz. The value of absorption loss in the atmospheric channel will vary from 0.98 dB at the elevation angle of 90° to 5.58 dB at the elevation angle of 10° for the signal frequency of 100 GHz. The transmitter antenna is considered as the parabolic reflector [47], whose gain can be found as $(\pi D/\lambda)^2$. The link-budget calculation is shown in the Appendix A for the given parameters.

The data for training and testing of the DNN beamformer are generated by varying the angle θ_0 from 0° to 80° in the steps of 0.1° . For each of these AoA, we vary the frequency of the received signal in the range of 99–101 GHz with a step size of 0.1 GHz and generate the corresponding DNN beamformer output voltage V_{out}^{DNN} . This creates 16,821 data samples for the training, testing and validation of the DNN beamformer. For each of these angles θ_0 and frequency of the received signal (99–101 GHz), we also obtain the output voltage of a TTD beamformer V_{out}^{TTD} . The network is then trained to minimize the MSE loss between these two output voltages over all the training samples. Each of the antenna elements has been assumed as an isotropic radiator with unity gain. The entire dataset is divided into a ratio of 70%, 15%, and 15% for training, validation and test respectively.

Table 1. Simulation Parameters.

Definition	Symbol	Value
Transmitter power	P_T	2 W
Transmitter antenna diameter	G_T	3 m
Satellite altitude	h_s	1000 km
Atmospheric height		100 km
Number of array elements	N	1000
Antenna efficiency	η_T, η_R	0.9
Center frequency	f_0	100 GHz
Antenna spacing at f_0	d	$0.5\lambda_0$
Bandwidth	B	2 GHz

The performance metric for the neural net is the mean square error between the output voltage of a TTD beamformer and the output of the DNN beamformer as shown in (10).

A neural network having 10 hidden layers with each layer consisting of 15 neurons is used for the design of DNN beamformer. The value of M i.e., the last layer of DNN is 15 and the value of K i.e., the number of training examples in our case corresponds to 11,775. The activation function for each of the neuron is tan-sigmoid function. The training algorithm uses Fletcher–Powell Conjugate Gradient method [48,49] to minimize the loss function over the training samples as defined in (10). In Figure 3, we show the out-of-sample performance of the proposed DNN beamformer with the output voltage (true) by a TTD beamformer and the output voltage predicted by the DNN beamformer. The sample number denotes samples selected from the generated data set that is reserved for testing. As we can observe, the DNN is able to track the performance as desired with a TTD beamformer at a given AoA θ_0 with very high accuracy.

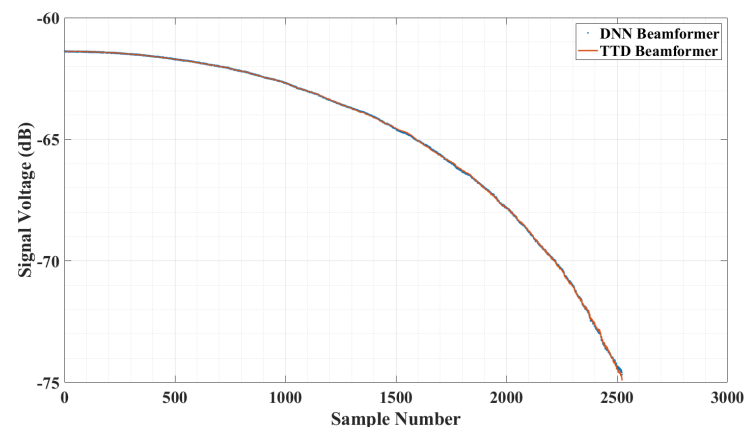


Figure 3. Output signal voltage predicted by the DNN beamformer and that of a true time delay beamformer for the test set at different angle of arrival θ_0 between $0\text{--}80^\circ$ for the considered frequency range of 99–101 GHz.

The MSE performance of the implemented DNN beamformer is shown in Figure 4 for the train, test and validation set. We can observe that the mean square (MSE) is very low thus showing that DNN is able to match the performance of a TTD beamformer as the AoA changes at the antenna array receiver. The best performance was obtained in 184 epochs with a very low mean square error as indicated in Figure 4. The MSE performance for the training, test and validation set was observed to be 9.73×10^{-13} , 10.005×10^{-13} and 9.64×10^{-13} respectively. Thus, as we can observe that for a wideband LEO satellite communication system, it is feasible to design a DNN beamformer that will replace the use of costly and non-ideal phase shifters for the beamforming of massive number of antenna array elements. The DNN is able to match the performance as expected by a TTD beamformer for a wideband LEO satellite communication system.

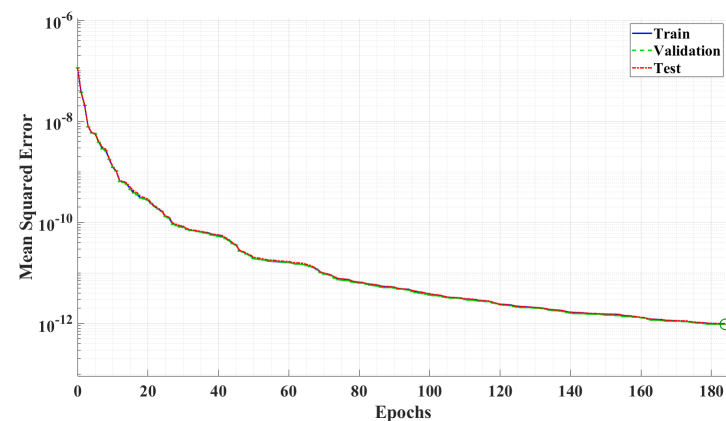


Figure 4. MSE Performance of proposed DNN Beamformer over the training, test and the validation dataset. The best MSE performance obtained at 184 epochs is indicated with a circle.

In order to compare and show the performance relative to the phase shifter implementation for a wideband signal, we show the signal voltage of the trained DNN, TTD and PSB beamformer at different frequencies in Figure 5 for the elevation angle in the range of 10–90°. The output of TTD is the ideal response that is desired for a wideband signal. It can be observed that for signal frequency of 100 GHz, the PSB also gives exact output as expected by a TTD beamformer but as the signal frequency deviates, the performance degrades severely. As pointed out earlier, this happens as the phase shifter is designed to provide specific delay at a given center frequency and as the frequency deviates, the phase response is not able to provide the constructive interference at the output. The spacing between the antenna elements at the center frequency is taken to be $0.5\lambda_0$. We note that the trained DNN beamformer is able to match the ideal performance as expected by a TTD beamformer as the elevation angle is varying in the range of 10–90°. As for massive number of array elements, the beamwidth of receiver antenna will be narrower and thus the effect of beam-squint can be severe.

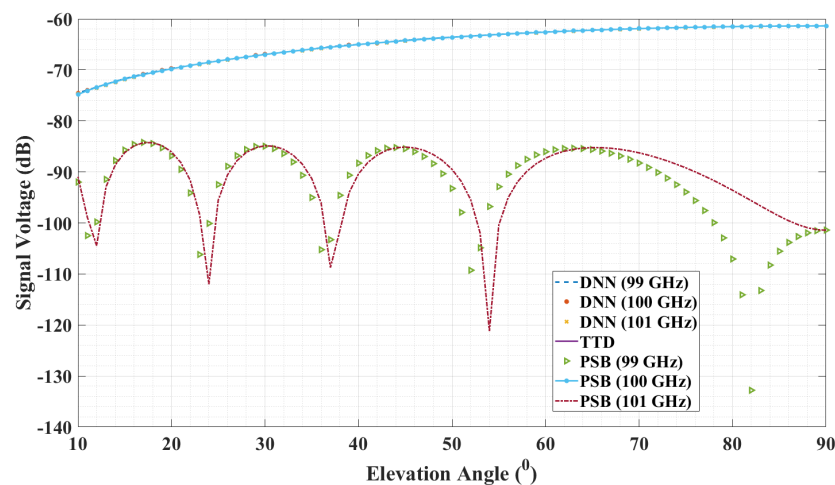


Figure 5. Performance comparison of PSB, TTD, and DNN Beamformer for the satellite elevation angle in the range of 10° to 90° at different frequencies of the wideband signal arriving at the antenna array.

4. Conclusions

In this work, we have proposed a DNN beamformer to implement the signal processing algorithm for a massive number of antenna array receiver at the ground station. It was shown that the proposed beamformer performs with very high accuracy for a wideband signal to match the output of a true time delay beamformer as the angle of arrival at the receiver array changes due to rapid movement of the LEO satellite. Such deployment of signal processing algorithm with a DNN beamforming will remove the use of phase shifters and the nonidealities caused by its implementation thus making it suitable for wideband communication systems. The implementation will lead to a highly efficient and low cost receiver design for wideband LEO satellite applications at sub-THz bands. In future, we will address the joint beamforming of multi-satellite station and ground station networks for optimal allocation of satellite resources in order to maintain high quality of service to the users.

Author Contributions: Conceptualization, R.K. and S.A.; Methodology, R.K. and S.A.; Writing—original draft, R.K. and S.A.; Writing—review & editing, R.K. and S.A.; Supervision, S.A. All authors have read and agreed to the published version of the manuscript.

Funding: This research received no external funding.

Acknowledgments: The authors would like to thank Kreitman School of Advanced Graduate Studies and Ben-Gurion University of the Negev, Israel for providing fellowships to continue the research. The authors would also like to thank the anonymous reviewers for their valuable suggestions to improve the article.

Conflicts of Interest: The authors declare no conflict of interest.

Appendix A

For the given link design parameters in Table 1, we provide the signal-to-noise ratio as the elevation angle of LEO satellite changes in Figure A1. The SNR at the receiver array output at the ground station would be expressed as [50]

$$SNR = \frac{\eta_R \eta_T P_T G_T G_R}{kTB L_{FS} L_A} \quad (A1)$$

where k is the Boltzmann constant, B is the bandwidth, T is the noise temperature, L_{FS} and L_A denote the free-space path loss and atmospheric absorption loss respectively. The value of noise temperature T_A is taken to be 500 K and the plot of SNR as a function of elevation angle is shown in Figure A1.

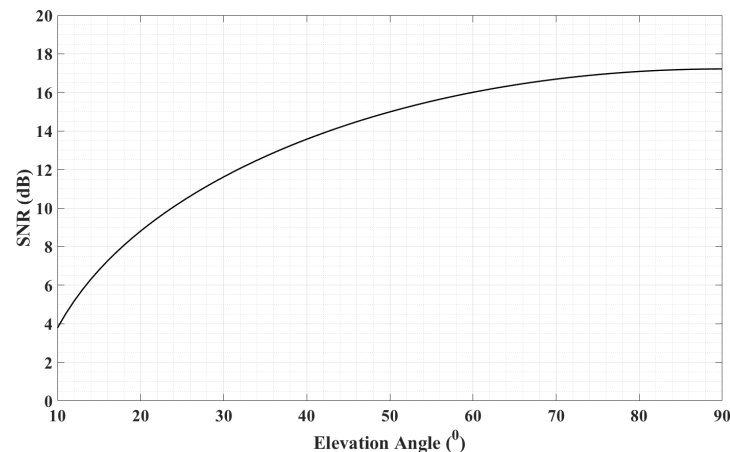


Figure A1. SNR of the LEO satellite link for the range of elevation angle varying from 10° to 90°.

We observe that the SNR is decreasing as the elevation angle is decreasing. This is expected as with lowering elevation angle, as the path length through the channel increases leading to higher absorption and free-space path loss. It should be noted that for a SNR of 4 dB, the bit-error rate (BER) of a Quadrature PSK (QPSK) would be 1.53×10^{-7} for the convolution coding with soft decision and code rate of 2/3. The simulation results have been shown up to the elevation angle of 10° as for the next-generation of LEO satellite networks, there will thousands of satellite in the orbit and the handover will be done at higher elevation angles to maintain high link quality [51].

References

1. Akyildiz, I.F.; Kak, A.; Nie, S. 6G and Beyond: The Future of Wireless Communications Systems. *IEEE Access* **2020**, *8*, 133995–134030. [CrossRef]
2. Božanić, M.; Sinha, S. Getting Ready for Terahertz Electronics. In *Millimeter-Wave Integrated Circuits: Methodologies for Research, Design and Innovation*; Springer International Publishing: Cham, Switzerland, 2020. [CrossRef]
3. 3GPP. 3GPP TR 38.811: Study on New Radio (NR) to Support Non-Terrestrial Networks. 2020. Available online: https://www.3gpp.org/ftp/Specs/archive/38_series/38.811/ (accessed on 26 October 2022).
4. 3GPP. 3GPP TR 38.821: Solutions for NR to Support Non-Terrestrial Networks (NTN). 2021. Available online: https://www.3gpp.org/ftp/Specs/archive/38_series/38.821/ (accessed on 26 October 2022).
5. 3GPP. 3GPP TR 36.763: Study on Narrow-Band Internet of Things (NB-IoT)/Enhanced Machine Type Communication (eMTC) Support for Non-Terrestrial Networks (NTN). 2021. Available online: https://www.3gpp.org/ftp/Specs/archive/36_series/36.763/ (accessed on 26 October 2022).

6. Kim, M.G.; Jo, H.S. Performance Analysis of NB-IoT Uplink in Low Earth Orbit Non-Terrestrial Networks. *Sensors* **2022**, *22*, 7097. [CrossRef]
7. Giordani, M.; Zorzi, M. Non-Terrestrial Networks in the 6G Era: Challenges and Opportunities. *IEEE Netw.* **2021**, *35*, 244–251. [CrossRef]
8. Shi, X.; Liu, R.; Thompson, J.S. Novel distributed beamforming algorithms for heterogeneous space terrestrial integrated network. *IEEE Internet Things J.* **2021**, *9*, 11351–11364. [CrossRef]
9. Lin, C.; Li, G.Y. Indoor Terahertz Communications: How Many Antenna Arrays Are Needed? *IEEE Trans. Wirel. Commun.* **2015**, *14*, 3097–3107. [CrossRef]
10. Lialios, D.I.; Ntetsikas, N.; Paschaloudis, K.D.; Zekios, C.L.; Georgakopoulos, S.V.; Kyriacou, G.A. Design of True Time Delay Millimeter Wave Beamformers for 5G Multibeam Phased Arrays. *Electronics* **2020**, *9*, 1331. [CrossRef]
11. Xiao, Z.; Han, Z.; Nallanathan, A.; Dobre, O.A.; Clerckx, B.; Choi, J.; He, C.; Tong, W. Antenna Array Enabled Space/Air/Ground Communications and Networking for 6G. *IEEE J. Sel. Areas Commun.* **2022**, *40*, 2773–2804. [CrossRef]
12. Ikram, M.; Sultan, K.; Lateef, M.F.; Alqadami, A.S.M. A Road towards 6G Communication: A Review of 5G Antennas, Arrays, and Wearable Devices. *Electronics* **2022**, *11*, 169. [CrossRef]
13. Dicandia, F.A.; Fonseca, N.J.G.; Bacco, M.; Mugnaini, S.; Genovesi, S. Space-Air-Ground Integrated 6G Wireless Communication Networks: A Review of Antenna Technologies and Application Scenarios. *Sensors* **2022**, *22*, 3136. [CrossRef]
14. García Sánchez, M. Millimeter-Wave Communications. *Electronics* **2020**, *9*, 251. [CrossRef]
15. Massacesi, A.; Dassano, G.; Pirinoli, P. Beam Scanning Capabilities of a 3D-Printed Perforated Dielectric Transmitarray. *Electronics* **2019**, *8*, 379. [CrossRef]
16. Amazon. Amazon’s Project Kuiper Satellites Will Fly on the New Vulcan Centaur Rocket in Early 2023. Available online: <https://www.aboutamazon.com/news/innovation-at-amazon/amazons-project-kuiper-satellites-will-fly-on-the-new-vulcan-centaur-rocket-in-early-2023> (accessed on 26 October 2022).
17. Rainbow, J. Lynk Global to Deploy Experimental 5G Payload in December. *SpaceNews*. Available online: <https://spacenews.com/lynk-global-to-deploy-experimental-5g-payload-in-december/> (accessed on 26 October 2022).
18. Pozdnyakov, A. iPhone 14 Will Have Satellite Connectivity. How Exactly It Will Work. *Universe Today*. Available online: <https://www.universetoday.com/157474/iphone-14-will-have-satellite-connectivity-how-exactly-it-will-work/> (accessed on 26 October 2022).
19. Liu, S.; Gao, Z.; Wu, Y.; Kwan Ng, D.W.; Gao, X.; Wong, K.K.; Chatzinotas, S.; Ottersten, B. LEO Satellite Constellations for 5G and Beyond: How Will They Reshape Vertical Domains? *IEEE Commun. Mag.* **2021**, *59*, 30–36. [CrossRef]
20. Bailleul, P.K. A New Era in Elemental Digital Beamforming for Spaceborne Communications Phased Arrays. *Proc. IEEE* **2016**, *104*, 623–632. [CrossRef]
21. Alzubaidi, O.T.H.; Hindia, M.N.; Dimiyati, K.; Noordin, K.A.; Wahab, A.N.A.; Qamar, F.; Hassan, R. Interference Challenges and Management in B5G Network Design: A Comprehensive Review. *Electronics* **2022**, *11*, 2842. [CrossRef]
22. Rappaport, T.S.; Xing, Y.; Kanhere, O.; Ju, S.; Madanayake, A.; Mandal, S.; Alkhateeb, A.; Trichopoulos, G.C. Wireless Communications and Applications Above 100 GHz: Opportunities and Challenges for 6G and Beyond. *IEEE Access* **2019**, *7*, 78729–78757. [CrossRef]
23. Pirapaharan, K.; Ajithkumar, N.; Sarujan, K.; Fernando, X.; Hoole, P.R.P. Smart, Fast, and Low Memory Beam-Steering Antenna Configurations for 5G and Future Wireless Systems. *Electronics* **2022**, *11*, 2658. [CrossRef]
24. Kumar, R.; Arnon, S. SNR Optimization for LEO Satellite at sub-THz Frequencies. *IEEE Trans. Antennas Propag.* **2022**, *70*, 4449–4458. [CrossRef]
25. Spoof, K.; Unnikrishnan, V.; Zahra, M.; Stadius, K.; Kosunen, M.; Ryyänen, J. True-Time-Delay Beamforming Receiver with RF Re-Sampling. *IEEE Trans. Circuits Syst. I Regul. Pap.* **2020**, *67*, 4457–4469. [CrossRef]
26. Rotman, R.; Tur, M.; Yaron, L. True Time Delay in Phased Arrays. *Proc. IEEE* **2016**, *104*, 504–518. [CrossRef]
27. Yang, G.; Zhang, Y.; Zhang, S. Wide-Band and Wide-Angle Scanning Phased Array Antenna for Mobile Communication System. *IEEE Open J. Antennas Propag.* **2021**, *2*, 203–212. [CrossRef]
28. Toledo, P.; Rubino, R.; Musolino, F.; Crovetti, P. Re-Thinking Analog Integrated Circuits in Digital Terms: A New Design Concept for the IoT Era. *IEEE Trans. Circuits Syst. II Express Briefs* **2021**, *68*, 816–822. [CrossRef]
29. Yang, B.; Yu, Z.; Lan, J.; Zhang, R.; Zhou, J.; Hong, W. Digital Beamforming-Based Massive MIMO Transceiver for 5G Millimeter-Wave Communications. *IEEE Trans. Microw. Theory Tech.* **2018**, *66*, 3403–3418. [CrossRef]
30. Peter, D.; Broughton, B.; Kraft, J. Phased Array Antenna Patterns—Part 2: Grating Lobes and Beam Squint. 2020. Available online: <https://www.analog.com/en/analog-dialogue/articles/phased-array-antenna-patterns-part2.html> (accessed on 26 October 2022).
31. Tanveer, J.; Haider, A.; Ali, R.; Kim, A. Machine Learning for Physical Layer in 5G and beyond Wireless Networks: A Survey. *Electronics* **2022**, *11*, 121. [CrossRef]
32. Luo, F.L.; Unbehauen, R. *Applied Neural Networks for Signal Processing*; Cambridge University Press: Cambridge, UK, 1998.
33. Rekkas, V.P.; Sotiroudis, S.; Sarigiannidis, P.; Wan, S.; Karagiannidis, G.K.; Goudos, S.K. Machine Learning in Beyond 5G/6G Networks—State-of-the-Art and Future Trends. *Electronics* **2021**, *10*, 2786. [CrossRef]
34. Luo, F.L.; Zhang, C.J. *Signal Processing for 5G: Algorithms and Implementations*; John Wiley & Sons: Hoboken, NJ, USA, 2016.
35. Dong, X.; Thanou, D.; Toni, L.; Bronstein, M.; Frossard, P. Graph Signal Processing for Machine Learning: A Review and New Perspectives. *IEEE Signal Process. Mag.* **2020**, *37*, 117–127. [CrossRef]

36. Jagannath, A.; Jagannath, J.; Melodia, T. Redefining Wireless Communication for 6G: Signal Processing Meets Deep Learning With Deep Unfolding. *IEEE Trans. Artif. Intell.* **2021**, *2*, 528–536. [[CrossRef](#)]
37. Ortiz-Gomez, F.G.; Lei, L.; Lagunas, E.; Martinez, R.; Tarchi, D.; Querol, J.; Salas-Natera, M.A.; Chatzinotas, S. Machine Learning for Radio Resource Management in Multibeam GEO Satellite Systems. *Electronics* **2022**, *11*, 992. [[CrossRef](#)]
38. Zhang, T.; Dong, A.; Zhang, C.; Yu, J.; Qiu, J.; Li, S.; Zhou, Y. Hybrid Beamforming for MISO System via Convolutional Neural Network. *Electronics* **2022**, *11*, 2213. [[CrossRef](#)]
39. Xia, W.; Zheng, G.; Zhu, Y.; Zhang, J.; Wang, J.; Petropulu, A.P. A Deep Learning Framework for Optimization of MISO Downlink Beamforming. *IEEE Trans. Commun.* **2020**, *68*, 1866–1880. [[CrossRef](#)]
40. Alkhateeb, A.; Alex, S.; Varkey, P.; Li, Y.; Qu, Q.; Tujkovic, D. Deep Learning Coordinated Beamforming for Highly-Mobile Millimeter Wave Systems. *IEEE Access* **2018**, *6*, 37328–37348. [[CrossRef](#)]
41. Li, W.; Huang, X.; Leung, H. Performance evaluation of digital beamforming strategies for satellite communications. *IEEE Trans. Aerosp. Electron. Syst.* **2004**, *40*, 12–26. [[CrossRef](#)]
42. ITU. ITU Recommendation P. 676-12: Attenuation by Atmospheric Gases and Related Effects. 2019. Available online: <https://www.itu.int/rec/R-REC-P.676> (accessed on 26 October 2022).
43. Silvestrini, S.; Lavagna, M. Deep Learning and Artificial Neural Networks for Spacecraft Dynamics, Navigation and Control. *Drones* **2022**, *6*, 270. [[CrossRef](#)]
44. Gao, J.; Zhong, C.; Li, G.Y.; Zhang, Z. Online Deep Neural Network for Optimization in Wireless Communications. *IEEE Wirel. Commun. Lett.* **2022**, *11*, 933–937. [[CrossRef](#)]
45. ITU. ITU Recommendation P. 835-6: Reference Standard Atmospheres. 2017. Available online: https://www.itu.int/rec/R-REC-P.835/_page.print (accessed on 26 October 2022).
46. Williams, C.R. How Much Attenuation Extinguishes mm-Wave Vertically Pointing Radar Return Signals? *Remote Sens.* **2022**, *14*, 1305. [[CrossRef](#)]
47. del Portillo, I.; Cameron, B.G.; Crawley, E.F. A technical comparison of three low earth orbit satellite constellation systems to provide global broadband. *Acta Astronaut.* **2019**, *159*, 123–135. [[CrossRef](#)]
48. Tansri, K.; Chansangiam, P. Conjugate Gradient Algorithm for Least-Squares Solutions of a Generalized Sylvester-Transpose Matrix Equation. *Symmetry* **2022**, *14*, 1868. [[CrossRef](#)]
49. Zhu, H.; Leandro, J.; Lin, Q. Optimization of Artificial Neural Network (ANN) for Maximum Flood Inundation Forecasts. *Water* **2021**, *13*, 2252. [[CrossRef](#)]
50. Kumar, R.; Arnon, S. Enhancing Cybersecurity of Satellites at Sub-THz Bands. In *Cyber Security, Cryptology, and Machine Learning*; Dolev, S., Katz, J., Meisels, A., Eds.; Springer International Publishing: Cham, Switzerland, 2022; pp. 356–365.
51. Deng, R.; Di, B.; Zhang, H.; Kuang, L.; Song, L. Ultra-Dense LEO Satellite Constellations: How Many LEO Satellites Do We Need? *IEEE Trans. Wirel. Commun.* **2021**, *20*, 4843–4857. [[CrossRef](#)]